ISSN: 1999-1630

SEU Journal of Science and Engineering, Vol. 13, No. 1, June 2018

Modelling of Performance Parameters of Single Photon Avalanche Detector Incorporating Dead Space Effects and History Dependent Ionization Coefficient

Azwad Tamir[1*] and Mohammad Shahriar Saif[2]

[1]Department of Electrical and Electronic Engineering, Southeast University, Dhaka, Bangladesh.
[2] Energypac Engineering Ltd, Dhaka, Bangladesh.

Abstract
The modelling and simulation of the performance parameters of single-photon avalanche diode (SPAD) is carried out with the help of MATLAB. The model is applied on a sample SAM SPAD device which consists of a multiplication region made of InP and an absorber region of InGaAs. A generalized theory for breakdown probability is implemented which takes into account the generation of photocarriers at random locations among each layer. The study reveals that by increasing the multiplication region width, the number of dark carriers due to field-assisted generation mechanisms is reduced which are counteracted by an increase in the number of GR dark carriers. Thus, the photon detection efficiency (PDE) and Dark count rate (DCR) is of utmost importance before the fabrication of a device. In this work we have simulated a SPAD device incorporating dead space effects and history dependent ionization coefficient to generate the electric field profile, dead space profile, ionization coefficient profile, breakdown profile and avalanche probabilities. Finally, we have extracted the PDE vs overbias voltage and PDE vs DCR curves of the simulated device under different multiplication region widths to demonstrate the effect of multiplication region width on the performance parameters of a SPAD.

Keywords: Dark Count Rate(DCR), Dead Space Multiplication Theory, History dependent Ionization Coefficient, Photo Detection Efficiency (PDE), Single Photon Avalanche Detector (SPAD).

I. Introduction

There can't be a smaller possible unit of light than a single photon. As a result, a photodetector with the ability to detect a single photon can be considered as the ultimate device for weak light detection (R. H. Hadfield, 2009). In modern times, single-photon detectors have already been used in a wide range of applications including Quantum information processing, Lidar, Photoluminescence and quantum communication. Almost all near-infrared SPDs can be classified into three major areas of devices: superconducting devices, photomultiplier tubes and semiconductor single-photon avalanche diodes (SPADs). Moreover, Single photon detection can be utilized in a wide range of new technologies including quantum dot resonant tunneling diodes and the quantum-dot optically gated field-effect transistor(E. J. Gansen *et al.*, 2007, J. C. Blakesley *et al.*, 2005).

Currently, the SPADs has established itself as the most viable candidate for single-photon light detection applications. A device is considered as an APD when it operates below the breakdown voltage in the linear-mode. In this type of device, the output photocurrent is linearly proportional to the input optical power. On the other hand, a photodiode is referred to as a SPAD when it is operated in the Geiger mode. Here, the biasing is kept above the breakdown voltage so that a self-sustaining avalanche in initiated with the absorption of just a single photon (J. Zhang *et al.*, 2015). A SPAD based detector system consists of two major parts: the SPAD device and the

* **Corresponding Author:** Azwad Tamir, Lecturer, Department of Electrical and Electronic Engineering, SouthEast University, 251/A & 252, Tejgaon I/A, Dhaka, Bangladesh; Email: *azwad.tamir@ieee.org*

quenching electronics. Therefore, the overall performance of a SPD system depends not only on the SPAD device, but on the quenching electronics as well (M. A. Itzler *et al.*, 2007).

The SPAD already dominates a wide region of widespread applications such as quantum key distribution (QKD), quantum teleportation, quantum secret sharing (QSS), quantum secure direct communication and counterfactual quantum cryptography (S. Cova *et al.*, 1996). And due to the rapid growth of SPAD performance, it is continually replacing other forms of photodetectors (A. Tosi *et al.*, 2009, A. K. Ekert, 1991).

The selection of proper performance parameters is an essential and crucial part any process (M. Hillery *et al.*, 1999). The simulated values of the different parameters would be useless no matter how accurate they are if they fail to represent and convey appropriate information about the attributes of the device under simulation (G. L. Long *et al.*, 2002). So, we went through significant literature of recent work related to SPAD performance to select the suitable parameters.

In the early years of the twenty first century a lot of attention was given in modeling the excess noise characteristics of the APDs. An essential parameter in estimating the excess noise characteristics of APDs hinges upon the accurate deduction of the ionization coefficient of the multiplication regions in the APDs.

Although the importance of the ionization coefficient is determining the excess noise characteristics of linear mode APD is experimentally supported, but due to the difference in working principle of the SPAD, the same parameters cannot be used in this case (D. A. Ramirez *et al.*, 2007). Many recent works emphasize the photon detection efficiency (PDE), the breakdown characteristics and the dark count probabilities to demonstrate the performance characteristics of SPAD (Z. Peng *et al.*, 2010).

Our work involves constructing a working simulator that can be used to determine the performance parameters in a single photon avalanche photodetector (SPAD). The first step was to select appropriate parameters that could be used to successfully and comprehensively describe the overall performance of a SPAD. The device selected was of a separate absorption multiplication and charging structure with InGaAs as the absorption region material, InP as the multiplication material and InGaAsP as the charging material placed in between the absorption and multiplication layers.

The next step was to construct the simulator in MATLAB® which takes the material specifications, different layer thickness, device geometry, history dependent ionization coefficients and operating voltages as input and generates the selected output parameters to provide a detailed analysis of the performance of the simulated device.

II. Model

In this section we will go through the details of the model employed to determine the performance parameters of a SPAD namely, the PDE and the DCR. The device that we have modeled is composed of separate absorption, charge and multiplication layers made out of InGaAs, InGaAsP and InP materials respectively. Light is incident from the bottom of the device so that most of the photons are absorbed in the absorption region of the device which has a lower electric field value as can be seen from figure 1. After absorption, the electron hole pairs are accelerated in the multiplication region with a very high electric field profile for creating an avalanche breakdown. The charge layer in between is placed to accommodate for the electric field gradient between the absorption and multiplication regions.

A schematic representation of our device is shown in figure 1, along with its corresponding electric field profile which was derived from

solving Poisson's equation. The dead space profile of holes and electrons are then calculated at different positions of the device. Figure 2 shows the dead space profile of a typical device consisting of a 1.5µm long absorption region and a 1.4µm long multiplication region operating at room temperature. The origin of the position axis is taken at the beginning of the P+ region.

The dead space profile becomes prominent when the multiplication region of the device falls to around 1µm in length and has to be included in the calculations to avoid errors.

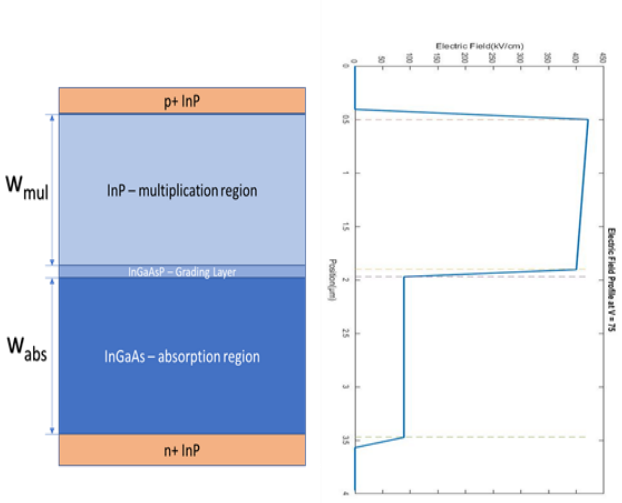

Figure. 1: Device structure and the electric field profile.

If we look at the relationship between the dead space length and the electric field, we would find that they are inversely proportional. It is greater in the absorption region compared to the multiplication region. Also increasing the bias voltage decreases the dead space considerably as can be seen in figure 2.

With the electric field known we drew upon existing models which finally led us to PDE and DCR values.

A. Photo Detection Efficiency:

We need to calculate the breakdown probabilities before we can find PDE and in order to do that we have to find the following profiles.

1) Dead Space Profile: In avalanche photodiodes (APD) and Single photon avalanche photodiodes (SPAD) newly generated carriers has to travel a certain amount

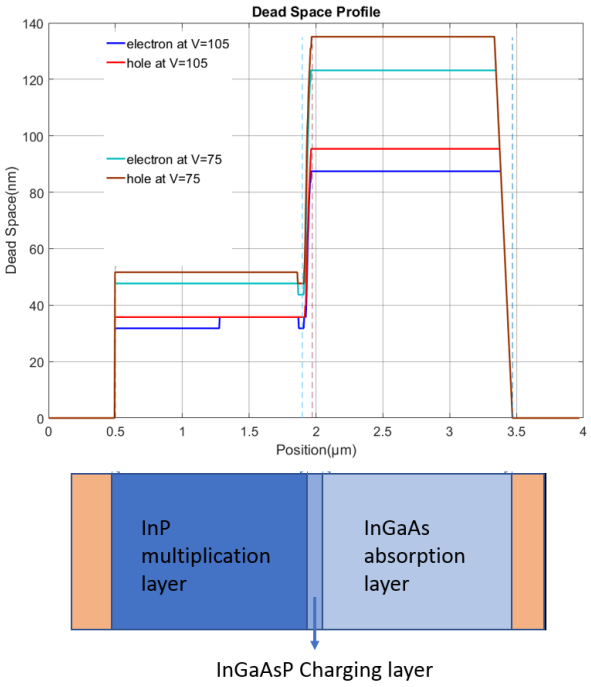

Figure. 2: Dead space profile for electrons and holes at V = 75V & 105V

of distance to gain sufficient energy to cause impact ionization. To take this effect into account Hayat *et al.* (M. M. Hayat *et al.*, 1992) formulated a model, where zero is set as the carrier's ionization probability for a certain distance, called the dead space right after the generation of the carrier.

$$E_{th,e}\left(x + d_e(x)\right) = q \int_{x}^{x+d_e(x)} E(u)\, du \qquad (1)$$

$$E_{th,h}\left(x - d_h(x)\right) = q \int_{x-d_h(x)}^{x} E(u)\, du \qquad (2)$$

The above equations are used to calculated the dead space profile of electrons and holes respectively where threshold energies, E_{th} have been found from literature (M. A. Saleh *et al.*, 2001, I. Watanabe *et al.*, 1995).

2) Prabability Density function: The ionization coefficients for InP are first calculated using the expression developed by

Zappa *et al.* (F. Zappa *et al.*, 1996), and find the ionization coefficients for InGaAs from Ng *et al.* (J. S. Ng *et al.*, 2003). Now that the ionization coefficients and dead space profiles are avalable the probability densiy functions is given by: (M. M. Hayat *et al.*, 2002).

$$h_e(\xi|x) = \begin{cases} \alpha(x+\xi)e^{-\int_{d_e(x)}^{\xi}\alpha(x+y)\,dy}, & \xi \geq d_e(x) \\ 0, & \xi < d_e(x) \end{cases} \tag{3}$$

$$h_h(\xi|x) = \begin{cases} \beta(x-\xi)e^{-\int_{d_h(x)}^{\xi}\beta(x-y)\,dy}, & \xi \geq d_h(x) \\ 0, & \xi < d_h(x) \end{cases} \tag{4}$$

Where $h_e(\xi|x)$ is the probability per unit distance that an electron born at location x impact ionize at ξ, while $h_h(\xi|x)$ has a similar definition.

3) Non-breakdown Probabilities: Let $P_{sh}(W|x)$ be the probability that an elctron born at x reaches the n+ region and Pse (0|x) the probability that a hole born at x reaches the p+ region. They can be defined as

$$P_{Se}(W|x) = e^{-\int_{x+d_e(x)}^{W}\alpha(x)\,dx} \tag{5}$$

$$P_{Sh}(0|x) = e^{-\int_{x-d_h(x)}^{0}\beta(x)\,dx} \tag{6}$$

We define $P_Z(x)$ as the probability that an electron born at x does not cause avalanche breakdown similarly, $P_Y(x)$ as the probability that a hole born at x does not case avalanche breakdown. From the model described by McIntyre (R. J. McIntyre, 1999) they can be written as

$$P_Z(x) = P_{Se}(W|x) + \int_0^{W-x} P_Z(x+\varepsilon)^2 P_Y(x+\varepsilon) h_e(\varepsilon|x)\,d\varepsilon \tag{7}$$

$$P_Y(x) = P_{Sh}(0|x) + \int_0^{x} P_Y(x-\varepsilon)^2 P_Z(x-\varepsilon) h_h(\varepsilon|x)\,d\varepsilon \tag{8}$$

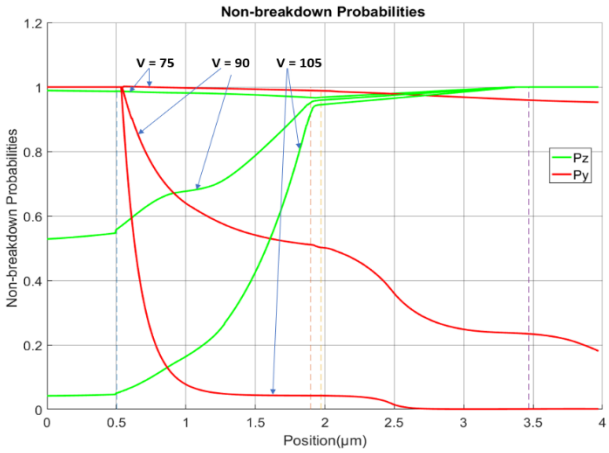

Figure. 3: Non-breakdown probabilities for electron (Pz) and hole (Py) at V = 75 V, 90V & 105 V.

Also, PA(x), the probability of avalanche at x can be written as

$$PA(x) = 1 - P_Z(x)P_Y(x) \tag{9}$$

Now by using the non-breakdown probabilities we can calculate the probability that an avalanche breakdown is triggered by an electron – hole pair photo-generated inside the absorption region, otherwise known as the injected carrier breakdown probability, Q_{ph} (D. A. Ramirez *et al.*, 2008)

$$Q_{ph} = \frac{-\ln(1-\eta)}{\eta w_{abs}} \int_0^{w_{abs}} e^{\frac{\ln(1-\eta)}{w_{abs}}x} \left(1 - P_Z(x)P_Y(x)\right)dx \tag{10}$$

where η is SPAD's quantum efficiency.

Finally, the photo detection efficiency can be defined as $PDE = \eta Q_{ph}$.

The non-breakdown probabilities of electrons and holes ($P_Z(x)$ and $P_Y(x)$) for a device with a 1.5μm long absorption region and a 1.4μm long multiplication region for different voltages is provided in figure 3. As the bias voltage is increased, the non-breakdown probabilities decrease. This is due to the fact that increasing the voltage increases the probability of breakdown and conversely decreases the non-probability. P_Z and P_Y plots are opposite in nature. This happens as

electrons and holes travel in opposite direction when an electric field is applied.

The electron travels from left to right, so the probability of an electron which is born more to the left to breakdown is more in comparison to another which is born further to the right. So the value of P_Z increases as we go toward the right. Also, the plot of avalanche probability versus position for the same device is given in figure 4.

B. Dark Current Rate

DCR is the count registered in absence of light and is a very important parameter for SPAD devices. There are mainly two sources of dark counts, thermal generation current and tunneling current.

Thermal generation current can be written as n_i/τ. Here τ is a material quality dependent property and we have used the value obtained by Donnelly *et al.* (J. P. Donnelly *et al.*, 2006), while the intrinsic carrier, n_i for each material are readily available.

Tunneling current itself has two categories: Direct Band to Band Tunneling and Tunneling through defect states. Current density of direct band to band tunnel is given by (J. L. Moll, 1964, S. M. Sze, 1981).

$$J_{tun\_Av\_dir}(x) = AE(x)^2 \exp\left(\frac{-BE_g{}^{1.5}}{E(x)}\right) \quad (11)$$

where, $A = q^3\left(2m_r/(qE_g)\right)^{1.5}/(4\pi^3\hbar^2)$,

$B = \pi\,(m_r/2)^{0.5}/(2q\hbar)$ and

$m_r = 2\,(m_c m_{lh})/(m_c + m_{lh})$

here $m_c$is the conduction band effective mass and m_{lh} is the light hole effective mass.

The tunneling through defect current density is given by (J. P. Donnelly *et al.*, 2006)

$$J_{tun\_Av\_def}(x) = \frac{AE(x)^2 N_T \exp\left(\frac{-B_1 E_{B1}{}^{1.5} - B_2 E_{B2}{}^{1.5}}{E(x)}\right)}{N_v \exp\left(\frac{-B_1 E_{B1}{}^{1.5}}{E(x)}\right) + N_c \exp\left(\frac{-B_2 E_{B2}{}^{1.5}}{E(x)}\right)} \quad (12)$$

where,

$B_1 = \pi\,(m_{lh}/2)^{0.5}/(2q\hbar)$, $B_2 = \pi\,(m_c/2)^{0.5}/(2q\hbar)$, E_{B1} is barrier height of tunneling from valence band to trap and E_{B2} is barrier height of tunneling from trap to conduction band.

The total current density is simply the sum of these two equations

$$J_{tun\_Av}(x) = J_{tun\_Av\_dir}(x) + J_{tun\_Av\_def}(x) \quad (13)$$

Finally, we can calculate DCR given by the equation:

$$DCR = \int_0^W \left(\frac{n_{i_{InP}}}{\tau_{InP}} + \frac{J_{tun_{Av}}(x)}{q}\right) PA(x)dx + PA(0)\left(\frac{n_{i\_abs}}{\tau_{abs}}\right) w_{abs} \quad (14)$$

III. Results

The PDE and DCR at different multiplication width are simulated to demonstrate the dependency of the performance parameters of a SPAD device on multiplication region width.

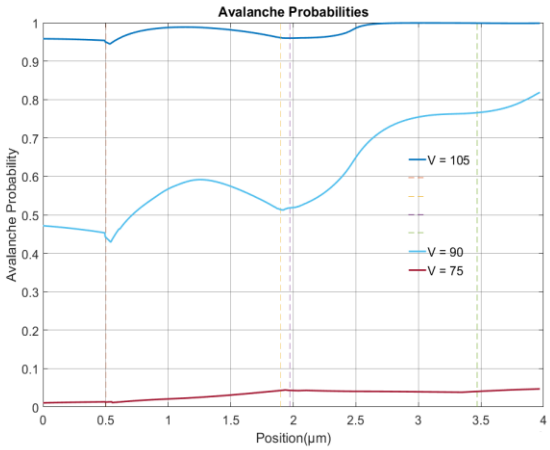

Figure. 4: Avalanche probabilities at V = 75 V, 90V & 105 V

The evaluation of this dependency is crucial prior to the fabrication of a device as this determines the optimum operating region of a device and indicates the fabrication parameters required for a particular application. The Non-breakdown probabilities: P_z for electrons and P_y holes have been calculated and simulated in MATLAB with the help of the model described

in the previous section. Next, the Avalanche probability at different layers and positions of the device is generated using equation 9 and shown in figure 4. Also, the value of the DCR at different multiplication region width and PDE are calculated, which is then used to simulate different PDE and DCR profiles of the device at various multiplication region width.

A plot of photo detection efficiency vs overbias at different multiplication region width is given in figure 5. As the voltage increases so does the PDE. But the PDE eventually attains saturation at a value of about

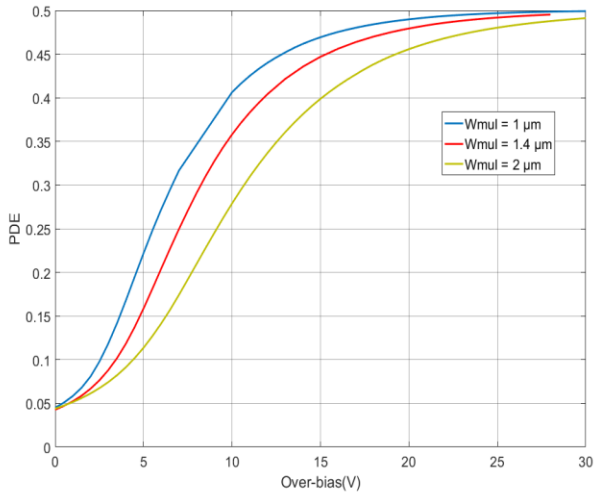

Figure. 5: Photo detection efficiency (PDE) at various multiplication region width.

"0.5". This occurs as the quantum efficiency used to calculate the PDE is taken to be "0.5". Increasing the multiplication region width eventually increases the voltage required to attain saturation. So, a larger multiplication region device requires a larger quenching circuitry, taking up more power and becoming less efficient.

Conversely, a lower multiplication region device has a larger DCR value compared to that with a larger multiplication region width as can be seen from figure 6. So, there exists a trade-off between the allowable DCR value and the operating voltage in a SPAD device. Lowering the multiplication region effectively decreases operating voltage and pressure on the external circuitry and increases efficiency. But, it also increases the DCR and there is a limit to the allowable DCR for a given external quenching circuitry used. Lowering the multiplication region width also increases the maximum operating temperature.

Before undertaking in the fabrication of a device for a specific application, it is of utmost importance to estimate the design parameters like the device dimensions and doping concentrations. This requires a functional simulator that can successfully predict the appropriate performance parameters given the design consideration as input. In order to comprehensively portray the performance of a SPAD device, a generalized model of the photo detection efficiency (PDE) and the Dark count rate (DCR) needs to be effectively constructed.

In the conventional ionization coefficient model for SPAD devices, the ionization coefficient was dependent on the electric field alone, this does not take into account the non-uniform electric field profile of heterostructure

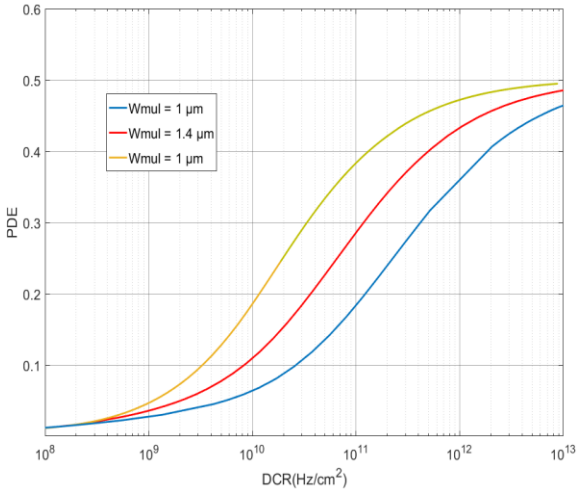

Figure. 6: PDE vs DCR for different multiplication region width.

Separate Absorption Multiplication (SAM) devices. To counteract this, we replaced the ionization coefficient with probability density functions (pdf) hh(y|x) and he(y|x) as proposed by McIntyre in 1999 (R. J. McIntyre, 1999).

Another shortcoming of the conventional model is its exclusion of the dead space as it was taken to be negligible in comparison to the multiplication region width, W_{mul}, of the SPAD. But due to the advancement of fabrication techniques in recent times, device fabrication with W_{mul} comparable to the dead space is possible. So, to preserve the generality of our model, the dead space incorporation technique proposed by Saleh *et al.* (M. A. Saleh *et al.*, 2001) was used to include the effects of dead space into an experimentally determined ionization coefficient (F. Zappa, 1996) to find out the dead incorporated pdf hh(y|x) and he(y|x). This pdfs along with the dead space profile and dark current model was combined to construct the PDE and DCR profiles of the device.

IV. Conclusion

We have simulated a detailed model of the SPAD performance parameters derived from basic principles which is nonspecific of device dimensions. So, a device of any shape and dimension can be simulated and the performance parameters accurately estimated using this model. The work can be further extended by adding other materials to the simulation so that devices made of materials other than InGaAs/InP can also be simulated.

The PDE vs overbias, DCR vs overbias and PDE vs DCR curves at variable multiplication width are generated. The value of PDE increases with applied voltage. But the PDE eventually attains saturation at a value of internal quantum efficiency. Increasing the multiplication region width eventually increases the voltage required to attain saturation. So, a larger multiplication region device requires a larger quenching circuitry, takes up more power and less efficient.

On the other hand, a lower multiplication region device has a larger DCR value compared to that with a larger multiplication region width. So, there exists a trade-off between the allowable DCR value and the operating voltage in an SPAD device. Lowering the multiplication region effectively decreases operating voltage and pressure on the external circuitry and increases efficiency. But, it also increases the DCR and there is a limit to the allowable DCR for a given external quenching circuitry used. The maximum operating temperature is also increased when the multiplication region is decreased.

References

A. K. Ekert, "Quantum cryptography based on Bell's theorem," *Physical Review Letters*, vol. 67, pp. 661-663, 1991.

A. Tosi, A. D. Mora, F. Zappa, S. Cova, "Single-photon avalanche diodes for the nearinfrared range: detector and circuit issues," *Journal of Modern Optics*, vol. 56, pp. 299-308, 2009.

A. Tosi, F. Acerbi, M. Anti, and F. Zappa, "InGaAs/InP Single-Photon Avalanche Diode with Reduced Afterpulsing and Sharp Timing Response with 30 ps Tail," *IEEE Journal of Quantum Electronics*, Vol. 48, No. 9, September 2012.

D. A. Ramirez, M. M. Hayat, M. A. Itzler, Dependence of the performance of single photon avalanche diodes on the multiplication region width: temperature and field effects, *IEEE Lasers and Electro-Optics Society Annual Meeting Conference Proceedings, Lake Buena Vista, FL,* pp. 511-512, Oct 2007.

D. A. Ramirez, M. M. Hayat and M. A. Itzler, "Dependence of the performance of single photonavalanche diodes on the multiplication region width", *IEEE Journal on Quantum Electron*, vol. 44, no. 12, pp. 1188–1195, Dec. 2008.

E. J. Gansen, M. A. Rowe, M. B. Greene, D. Rosenberg, T. E. Harvey et al, "Photon-number discriminating detection using a quantum-dot, optically gated, field-effect transistor", *Nat Photonics*, pp. 585-588, 2007.

F. Zappa, P. Lovati, A. Lacaita, "Temperature dependence of electron and hole ionization coefficients in InP", *Proc. IPRM*, pp. 628-631, 1996.

G. L. Long, X. S. Liu, "Theoretically efficient high-capacity quantum-key-distribution scheme," *Physics Review A*, pp. 65, 2002.

I. Watanabe, T. Torikai and K. Taguchi, "Monte Carlo Simulation of Impact Ionization Rates in InAlAs-InGaAs Square and Graded Barrier Superlattice", *IEEE Journal of Quantum Elecronics*, vol. 31, pp. 1826-1834, 1995.

J. C. Blakesley, P. See, A. J. Shields, B. E. Kardyna, P. Atkinson et al, "Efficient single photon detection by quantum dot resonant tunneling diodes", *Physical Review Letters, pp. 94*, 2005.

J. S. Ng, C. H. Tan and J. P. R. David, "Field Dependence of Impact Ionization Coefficients in $In_{0.53}Ga_{0.47}As$", *IEEE Transaction Electron Devices*, vol. 50, pp. 901-905, 2003.

J. Zhang, M. Itzler, H. Zbinden and J. Pan, "Advances in InGaAs/InP single-photon detector systems for quantum communication", *Light: Science & Applications*, vol. 4, no. 5, pp. e286, 2015.

M. A. Itzler, R. B. Michael, C. F. Hsu, K. Slomkowski, A. Tosi, *et al.*, "Single photon avalanche diodes (SPADs) for 1.5 mm photon counting applications," *Journal of Modern Optics*, vol. 54, pp. 283-304, 2007.

M. A. Saleh, M. M. Hayat, P. Sotirelis, A. L. Holmes, J. C. Campbell, B. E. A. Saleh, and M. C.Teich, "Impact-ionization and noise characteristics of thin III-V avalanche photodiodes," *IEEE Transaction Electron Devices*, vol. 48, pp. 2722–2731, 2001.

M. Hillery, V. Buzˇek, A. Berthiaume, "Quantum secret sharing," *Physical Review A*, vol. 59, pp. 1829-1834, 1999.

M. M. Hayat, B. E. A. Saleh and M. C. Teich, "Effect of dead space on gain and noise of doublecarrier-multiplication avalanche photodiodes", *IEEE Transaction on Electron Devices*, vol. 39, pp. 546-552, 1992.

M. M. Hayat, O.-H. Kwon, S. Wang, J. C. Campbell, B. E. A. Saleh, and M. C. Teich, "Boundary effects on multiplication noise in thin heterostructure avalanche photodiodes: Theory and experiment", *IEEE. Transaction on Electron Devices*, vol. 49, no. 12, pp. 2114–2123, 2002.

R. H. Hadfield, "Single-photon detectors for optical quantum information applications", *Nat Photonics*, pp. 696-705, 2009.

R. J. McIntyre, "A new look at impact ionization—Part I: A theory of gain, noise, breakdown probability, and frequency response", *IEEE Transaction Electron Devices*, vol. 46, pp. 1623–1631, 1999.

S. Cova, M. Ghioni, A. Lacaita, C Samori, F. Zappa, "Avalanche photodiodes and quenching circuits for single-photon detection," *Journal of Applied Optics*, vol. 35, pp. 1956-1976, 1996.

Z. Peng, Li Chun-Fei, L. Chang-Jun, W. Zheng-Jun, Y. Shu-Qiong, "Numerical analysis of In0.53Ga0.47As/InP single photon avalanche diodes", *Chinese Physics B*, vol. 20, 028502, 2010.